Materials Research. 2019; 22(3):e20180623
DOI: http://dx.doi.org/10.1590/1980-5373-MR-2018-0623

F-127-Assisted Sol-Gel Synthesis of Gd_2O_3:Eu^{3+} Powders and Films

***Antonieta García Murillo*[a]*, *Víctor Hugo Colín Calderon*[a], *Felipe de Jesús Carrillo Romo*[a], *Dulce Yolotzin Medina Velázquez*[b]**

[a]*Instituto Politécnico Nacional, Centro de Investigación e Innovación Tecnológica CIITEC, Cerrada de Cecati S/N. Col. Santa Catarina, Azcapotzalco, 02250 CDMX D. F., México*
[b]*División de Ciencias Básicas e Ingeniería, Universidad Autónoma Metropolitana-Azcapotzalco, Av. San Pablo No 180, C.P. 02200, Col. Reynosa-Tamaulipas, México*

Received: September 18, 2018; Revised: February 08, 2019; Accepted: February 20, 2019

In the current work, the influence of Pluronic F-127 (S = F-127) and temperature on the luminescent properties of Gd_2O_3:Eu^{3+} (Gd:S = 1:2) powders and films was studied. In order to synthesize the powders and films (by the dip-coating technique), Gd_2O_3: Eu^{3+} (5 mol%) ceramics were elaborated by the sol-gel route, using gadolinium and europium nitrates as precursors. The results obtained by means of X-ray diffraction, confirmed the presence of the cubic structure of Gd_2O_3 (in 800 ºC heat-treated powders and 700 ºC heat-treated films), and crystals with nanometer sizes of ~19 nm, and ~15 nm, corresponding to the spherical and laminar-like morphologies of densified powders and films, respectively. Crystallites from the cubic and monoclinic structure were present on Gd_2O_3: Eu^{3+}-modified films up to 800 ºC. Chemical identification of the bonds present in the films was performed by Fourier transform infrared spectroscopy, which identified representative infrared absorption at 543 cm^{-1}, attributable to the Gd-O vibration. Photoluminescence studies showed that when the powders and films were heat-treated at 800 ºC, the intensity of their luminescence at the $^5D_0 \rightarrow {}^7F_2$ Eu^{3+} transition (618 nm) was enhanced by the presence of F-127.

Keywords: *Gd_2O_3, Pluronic F-127, sol-gel, powders, films, europium.*

1. Introduction

The luminescence of rare earth (RE)-doped oxides (Ln_2O_3, Ln = RE) has been of great interest in recent decades, due to their applications in optoelectronic devices and to their sufficient brightness, high chemical stability, low phonon energy, and long-term stability [1,2,3]. Specifically, Gd_2O_3, considered an appropriate matrix for doping with europium due to its good luminescent characteristics and low phononic energy, presents a characteristic emission at 612 nm, corresponding to the transition $^5D_0$ - $^7F_2$ in the Eu used in panel display devices, such as PDPs [4], electroluminescent devices (ELDs) [5], fluorescent lamps [6], and so forth. Surfactant-modified Gd_2O_3:Eu^{3+} systems are promising alternatives for practical applications involving the development of nanodevices [7]. Moreover, the luminescent properties of these systems depend on their morphology, size, and synthetic route [8]. There are several methods for preparing Gd_2O_3: Eu^{+3}, such as by the combustion [9], Pechini [10], sol-gel [11,12], polyol [13,14] and hydrothermal [15] methods, as well as others, giving rise to different morphologies and particle sizes, making it possible to modify the intensity of the luminescent emissions.

Some reports point to nanoflowers particles as promising candidates for applications in field emitters because of their thin open edges [16]. In this work, we report on the synthesis of Gd_2O_3:Eu^{3+} powders and films modified with a surfactant (Pluronic F-127) by the sol-gel route, and on their influence on emission properties.

Their influence of Gd_2O_3:Eu^{3+} on structural and morphological characteristics was analyzed by infrared spectroscopy (FTIR), X-ray diffraction, and SEM, and the emission characteristics of the as-prepared powders and films were investigated using photoluminescence.

2. Experimental

2.1 Synthesis of Gd_2O_3:Eu^{3+} with F-127 surfactant

Gd_2O_3: Eu^{3+} powders and films synthesized in the presence of F-127 were prepared using gadolinium nitrate $Gd(NO_3)_3$ (99.9% Signa Aldrich), ethanol (C_2H_6O) (Fermont 99.9%), and europium (III) nitrate ($Eu(NO_3)_3$) (99.9% Alfa Aesar). The molar composition of the sol was Gd:Eu:C_2H_6O = 1:0.18:0.038. The gadolinium nitrate was dissolved in ethanol for 15 min. Thereafter, europium nitrate was added to the gadolinium sol under vigorous stirring at room temperature for 1 h in order to get the desired concentration (5 mol% Eu^{3+}). The established Eu was used because concentration quenching may occur in heavily Eu^{3+}-doped systems, arising from the distance-dependent, non-radiative, cross relaxation between neighboring Eu^{3+} ions [17]. In order to prepare surfactant-modified Gd_2O_3:Eu^{3+} systems, F-127 (monomer atomic

* e-mail: angarciam@ipn.mx

weight = 102 $gmol^{-1}$, Sigma Aldrich) chemical modifier precursor was added to the stable europium-doped gadolinium sol. Both compounds were dissolved (Gd:S=1:2) at room temperature in a dry box under nitrogen flux (humidity level < 3%). The europium-doped modified gadolinium solution was filtered through 0.2 µm and deposited on carefully cleaned pure silica substrates using the dip-coating technique [18] with a withdrawal speed of 80 mm min^{-1}, in order to obtain six layers. The layers were heat treated at 350 ºC for 30 min between each coating. The Gd_2O_3:Eu^{3+} precursor solutions were dried at 100 ºC for 24 h. The processed powders and films were finally annealed in air for 1 h at the required temperatures, ranging from 300 to 800 ºC. Crack-free and transparent layers were obtained and studied at room temperature. Both Gd_2O_3:Eu^{3+} powders and films without F-127 were prepared for the purpose of comparison.

2.2 Experimental techniques

Fourier transform medium infrared (FTIR) spectrograms were recorded using a Perkin-Elmer Spectrum 65, in a range of 4000-400 cm^{-1}, using the KBr pelleting technique. X-ray diffraction (XRD) patterns were recorded at room temperature on a PANalytical θ/θ Bragg Brentano X´Pert MPD PRO diffractometer, with a Cu Ka beam at 40 kV, 20 mA over a 2-θ range of 20º-80º (0.1º/s). The structural properties were also investigated by FTIR (Lambda 2000 Spectrum One, Perkin Elmer) spectroscopy. Scanning electron microscopy (SEM) was performed on the samples with a JEOL JSM-7800F microscope operated at 15 kV. The emission spectra were measured at room temperature with a Hitachi F-7000 spectrophotometer equipped with a 150-W xenon lamp as the excitation source.

3. Results and Discussion

3.1 Structural and morphological characterization of Gd $_2O_3$:Eu^{3+}/F-127 powders and films

The X-ray diffraction patterns of the Gd_2O_3:Eu^{3+} (5 mol%) powders and films heat-treated at temperatures ranging from 300 to 800 ºC and synthesized with F-127 are depicted in Fig. 1a and Fig. 1b, respectively. Fig. 1c shows the X-ray diffraction patterns of the Gd_2O_3:Eu^{3+} (5 mol %) powders and films heat-treated at 800 ºC and synthesized without F-127.

Four main characteristic peaks are clearly observable in the XRD patterns in Fig. 1a at a temperature of 800 ºC.

The observed peaks at (2 2 2), (4 0 0), (4 3 1), (4 4 0), (6 1 1), and (6 2 2) correspond to the characteristic reflection lines of gadolinium oxide powders crystallized into the cubic phase (JCPDS 12-0797). As the temperature decreased, the diffraction intensity remained stable up to 500 ºC, when crystallization started. At lower temperatures, the presence of the band observed around 30º is associated with the presence of an amorphous phase. The sharp and strong peaks demonstrate the high crystallinity exhibited by the Gd_2O_3 samples.

The XRD patterns of the as-prepared films heat-treated at different temperatures (Fig. 1b) show the transformation up to 600 ºC, corresponding to all Bragg reflections, according to standard data on the cubic phase. No peaks, shifts, or other phases appear in the presence of F-127 surfactant up to 700 ºC and 800 ºC for the films and powders, respectively that indicates the high purity of the precursors and their complete conversion to Gd_2O_3:Eu^{3+} at 600 ºC in the cubic phase. Nevertheless, some of the relative peak intensities are very different; this may be due to the <100> preferred orientation exhibited by the films [19]. However, a previous report on Gd_2O_3 without F-127 does not show this behavior [20]. Cho et al. demonstrated that preferential orientation occurs when the film grown by nucleation at the lowest strain energy [21]. An interesting change occurs in Gd_2O_3:Eu^{3+}-modified surfactant films-some peaks associated with the monoclinic phase (JCPDS 43-1015) occur at 800 ºC; this effect is probably due to the presence of nanoclusters [22], with some residual stress [23]. This behavior has not been shown for Eu-doped Gd_2O_3 modified surfactant films in previous reports.

In both cases, the presence of doping concentrations of Eu ions in the Gd_2O_3 structure (with a similar electric charge) indicates that Eu^{3+} was uniformly incorporated into the host lattice by substitution. This was due to the fact that the ionic radii for both lanthanide ions were almost the same (0.938 Å for Gd^{3+}, 0.947Å for Eu^{3+}) [24], which did not affect the host structure of the Gd_2O_3. Finally, the C-type structure of Gd_2O_3 offers two nonequivalent sites for lanthanide doping ions: C_2 (non-centrosymmetric) and S_6 (centrosymmetric). In both crystalline structures, the coordination environment of the lanthanide doping ions occupying the two possible sites is C_2:S_6 = 3:1 [25].

The crystallite sizes of both cubic systems (powders and films in the presence of F-127) were simulated, taking into account a Rietveld refinement. The size of the coherent domains was derived from a refinement of the full-width at half-maximum (FWHM), β, of the patterns fitted with pseudo-Voigt functions, according to the following relations [26]:

$$\beta^2 = IG/(\cos^2\theta),$$

where IG is a measure of the isotropic size effect

$$d = (180K\lambda)/\pi\sqrt{IG}$$

where d = the size [Å], λ = wavelength [Å], and K, the Scherrer constant, is equal to 4⁄3.

Fig. 1d shows the evolution of the crystallite sizes of the Gd_2O_3:Eu^{3+} powders and films as a function of temperature, compared to the Gd_2O_3:Eu^{3+} particles synthesized without F-127. These values were found to increase as the temperature

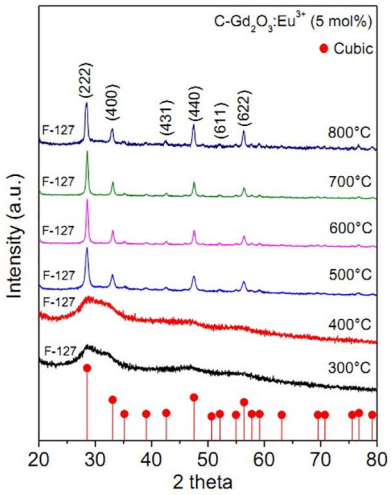

(a) powders synthesized with F-127 and heat-treated at different temperatures

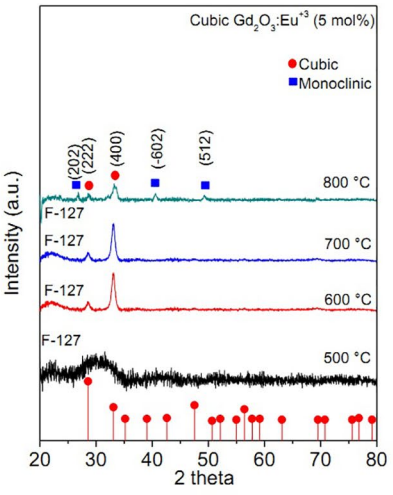

(b) films synthesized with F127 and heat-treated at different temperatures

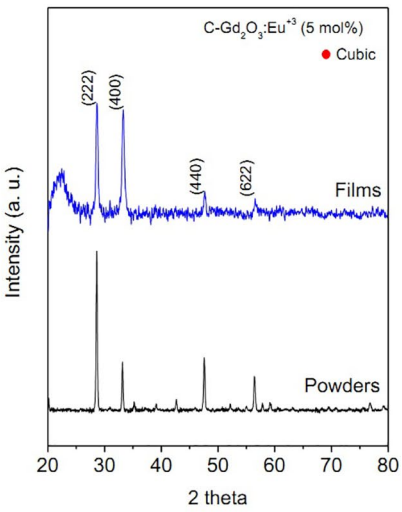

(c) powders and films synthesized without F127 and heat-treated at 800 °C

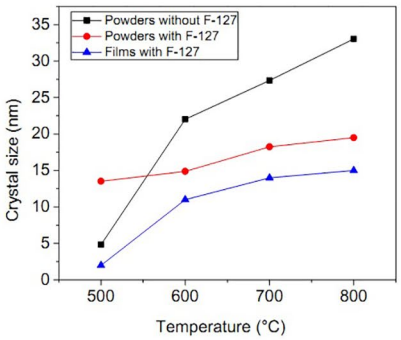

(d) crystallite sizes for Gd2O3:Eu3+ powders synthesized with and without F-127 and for films in presence of F-127 at different temperatures

Figure 1. X-ray diffraction patterns of $Gd_2O_3:Eu^{3+}$ (a) powders, (b) films synthesized with F127 and heat-treated at different temperatures, (c) powders and films synthesized without F127 and heat-treated at 800 ºC, (d) crystallite sizes for $Gd_2O_3:Eu^{3+}$ powders synthesized with and without F-127 and for films in presence of F-127 at different temperatures.

increased; at 800 ºC, the crystallite size for the reference powders corresponded to the largest one, at 33 nm. For samples synthesized in the presence of F-127 and heat-treated at 800 ºC, the crystal sizes observed for the powders and films were 19 nm and 15 nm at the highest temperature. It has been observed that the influence of F-127 on nanophosphors provokes an increment in particle dispersion, blocking the growth of the nanoparticles and modifying their shape and size [27,28].

In accordance with previous reports, the non-modified and F-127-modified Eu^{3+}-doped Gd_2O_3 systems exhibited two important features: (1) there is evidence of some reflection associated with the monoclinic phase in densified films (at 800 ºC) and (2) the preferred orientation was observed only

in the F-127-modified Gd_2O_3 sol-gel films, but not in the non-modified films or powders (Fig. 1c). These effects were produced by the presence of an organic additive, causing a reduction of the strain energy involved in the nucleation growth [29].

3.2 FTIR studies

Fig. 2 shows the normalized FTIR spectra of the 5 mol% Eu-doped Gd_2O_3 powders synthesized in the presence of F-127, annealed from 600 to 800 ºC. The broad bands situated around 3500 cm^{-1} and 1650 cm^{-1} arise from the absorption of O-H stretching (ν) and O-H deformation (δ) vibrations. The peaks in the wavelength range from 1510 to 1390 cm^{-1} assigned to NO_3 group (from gadolinium precursor) and the symmetric and asymmetric C=O vibrations [30]. All of these intensity bands decreased as the annealing temperature increased and were practically eliminated at 700 ºC, due to evaporation of absorbed water and -NO_3 gases. Nevertheless, the heat-treatment at air atmosphere was not enough to eliminate NO_3 group, but a combined annealing in vacuum and air atmosphere is more efficient to remove remaining organic molecules [31]. A sharp peak associated with this ligand at 1384 cm^{-1} was observed even after 700 ºC heat treatment. The bands around 544 cm^{-1} and 438 cm^{-1} are due to the characteristic (Gd-O) stretching vibrations of cubic Gd_2O_3 [32,33].

These characteristic bands were observed for the powders heat-treated up to 500 ºC, suggesting that the crystallization process was just starting at this temperature. The Gd_2O_3:Eu^{3+} powders present an amorphous phase at temperatures lower than 500 ºC, in agreement with the XRD results.

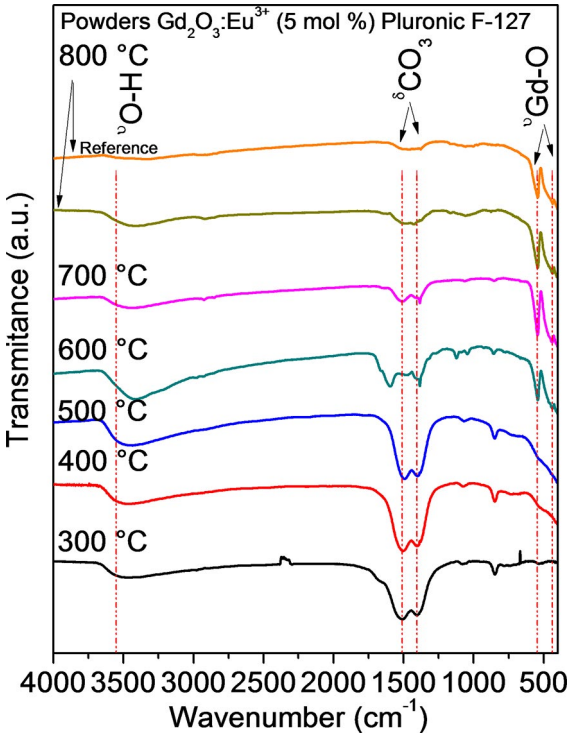

Figure 2. IR spectra of the Gd_2O_3:Eu^{3+} powders synthesized in the presence of F-127.

3.3 Morphological characteristics

In order to examine the morphology of the Gd_2O_3:Eu^{3+} ceramics and establish the influence of Pluronic F-127 on powders and films, the as-prepared samples were analyzed by means of the SEM technique.

Figs. 3a and d show SEM micrographs of the Gd_2O_3:Eu^{3+} powders and films without F-127, heat-treated at 800 ºC for 1 h. The Gd_2O_3:Eu^{3+} powders synthesized without F-127 (Fig. 3a) exhibit a flower shape 4 μm in size. In the case of the Gd_2O_3:Eu^{3+} films synthesized without F-157 (Fig. 3b), the SEM image reveals a homogeneously dispersed surface constituted by closely packed particles, radially distributed and less than 250 nm in size.

Fig. 3c and d show zones of the Gd_2O_3:Eu^{3+} powders and films, respectively, synthesized in the presence of F-127. The morphology of the europium-doped powders reveals a mix of homogeneous spherical particles, well distributed, of approximately 1 and 4 μm in size. The morphological analysis of the Gd_2O_3:Eu^{3+} films with Gd:S = 1:2 revealed a porous surface with round particles promoted by the high F-127 concentration in the layers [34]. It is well known that the presence of this molecule (F-127) in the sol plays a crucial role in synthesizing surfactant-modified ceramic films. Surfactants like F-127 reduce the hydrolysis and condensation reaction rates, due to the capping effect of F-127 on the metal precursor [35,36]. This molecule is used to prepare rough and mesoporous surfaces for a number of applications [37]. The established surfactant concentration F-127/Gd = 2 seems to determine the collapse of the inorganic ceramic being synthesized, producing a greater number of interstices between particles/aggregates, seemingly a consequence of removing the surfactant molecules before the calcination step.

3.4 Luminescent properties

Figs. 4and 5 show the PL spectra of Gd_2O_3:Eu^{3+} synthesized in the presence of F-127 as a function of temperature (Figs. 4a and 5a), and comparisons between the as-prepared systems synthesized with and without F-127, heat-treated at 800 ºC (Figs. 4b and 5b).

The emissions arising from the powders (Fig. 4) and films (Fig. 5) are characterized by an intense emission peak situated at 612 nm. Five groups of emission lines are assigned to $^5D_0 \rightarrow {}^7F_J$ (J = 0, 1, 2, 3), being the most intense the $^5D_0 \rightarrow {}^7F_2$ transition, an electric dipole-allowed transition that is hypersensitive to the environment. This strong emission occurs when Eu^{3+} ions occupy the sites without inversion centers inside the host lattice. Fig. 4a (the powders) and Fig. 5a (the films) show the emission spectra for Gd_2O_3:Eu^{3+} synthesized in the presence of F-127, heat-treated from 300 to 800 ºC. The luminescence intensity of the Eu^{3+}-modified

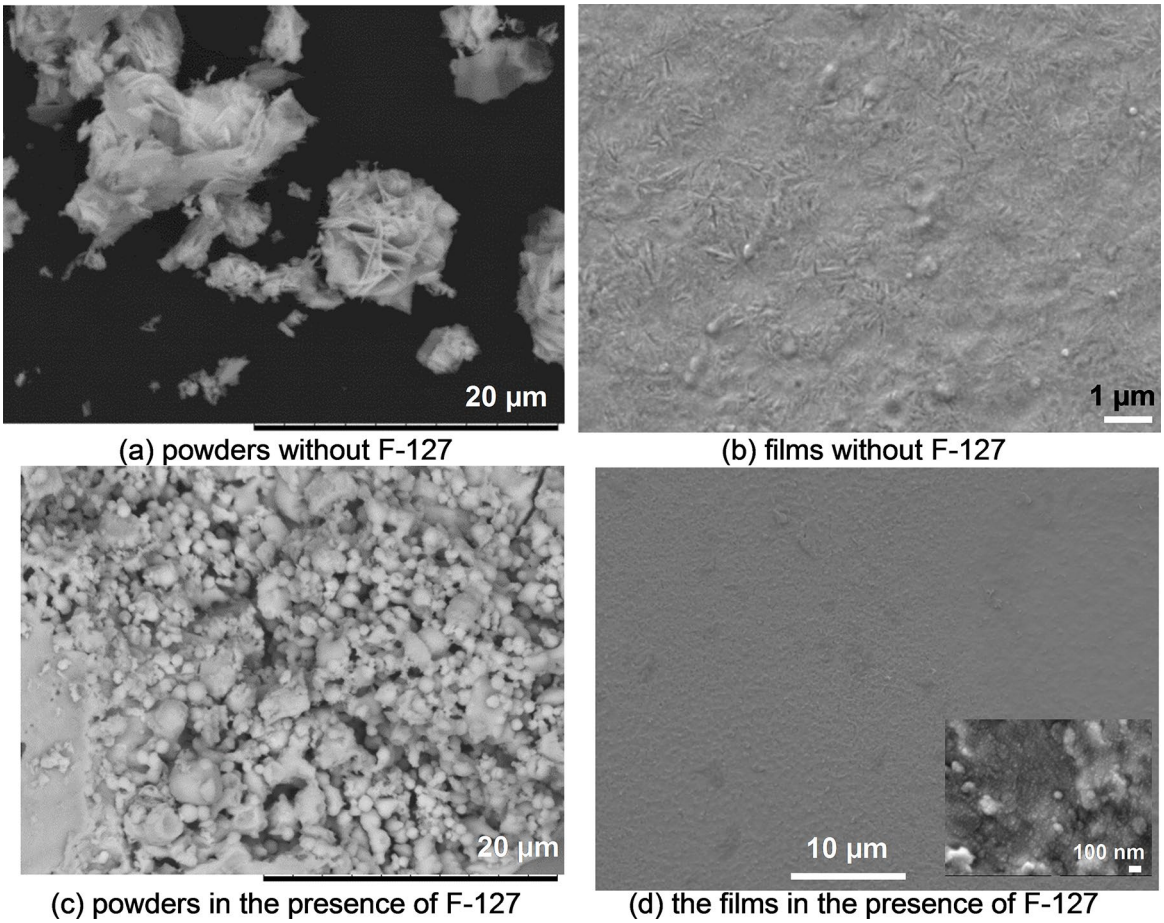

Fig. 3. SEM micrographs of (a) the $Gd_2O_3:Eu^{3+}$ powders and (b) the films without F-127, and (c) the $Gd_2O_3:Eu^{3+}$ powders and (d) the films in the presence of F-127.

powders increases with an increase in temperature and improves crystallization. A poor emission intensity was observed for the $Gd_2O_3:Eu^{3+}$ /F-127 powders at temperatures lower than 600 ºC that may be associated with the presence of an amorphous phase for systems annealed at up to 500 ºC.

The effects of temperature on the luminescence properties of both powders and films with and without F-127 were analyzed and compared at 800 ºC. Fig. 4b (the powders) and Fig. 5b (the films) reveal an intensity improved by the presence of the surfactant. These results can be explained by a better densification process and by less associated grain boundary absorption, reducing internal reflections of the emitted light due to rougher surfaces [38]. In the case of the $Gd_2O_3:Eu^{3+}$ films annealed at different temperatures, differences can be observed regarding the $^5D_0 \rightarrow {}^7F_0$ (581-nm) and $^5D_0 \rightarrow {}^7F_1$ (splits at 588, 592 and 599 nm) transitions, because they represent the local environment of the Eu^{3+}. For the F-127-modified and non-modified films heat-treated at 800 ºC, the sharp lines located at 581, 588, 592 and 599 nm (Fig. 5b) are associated with the $^5D_0 \rightarrow {}^7F_1$ transition, this one is magnetic-dipole-allowed; its intensity shows small variations, with a crystal field strength close to that of the Eu^{3+} ions.

Nevertheless, for the $Gd_2O_3:Eu^{3+}$ in the presence of F-127 heat-treated films at temperatures lower than 800 ºC, these bands are weaker and broader than those observed for modified films thermally treated at 800 ºC. This discrepancy between the emission peaks cannot be attributed to the presence of particles crystallized into the monoclinic phase (Fig. 1b); rather, the existence of mixed cubic and monoclinic phases could induce a spectroscopic adjustment, because the most intense peak, at $^5D_0 \rightarrow {}^7F_2$, shows a red shift in the non-modified and F-127-modified films, centered at 611.8 nm and 612.4 nm, respectively. This effect indicates that the emissions obtained from the modified films came from the presence of monoclinic particles aside from cubic ones, with a maximum emission peak at a longer wavelength and blue-shifted for only the cubic nanoparticles [39]. A small fraction of the monoclinic nanocrystallites present in the modified $Gd_2O_3:Eu^{3+}$ films failed to produce a luminescent signal, due to the monoclinic environment, because the peaks seen in the emission spectrum of the modified film are narrower and upshifted by the cubic structure. This result shows that the

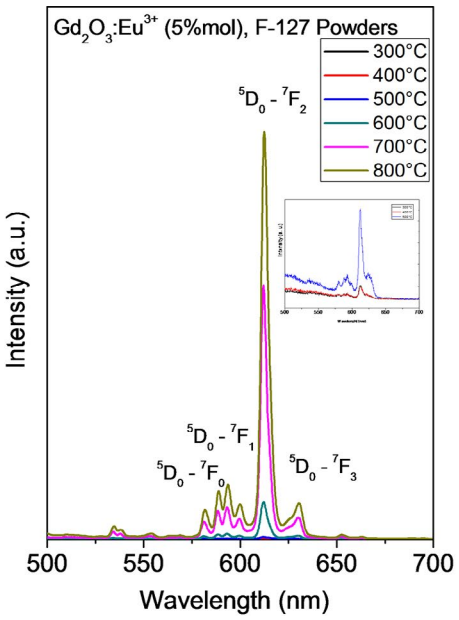

(a) the $Gd_2O_3:Eu^{3+}$ powders synthesized in the presence of F-127 heat-treated at different temperatures

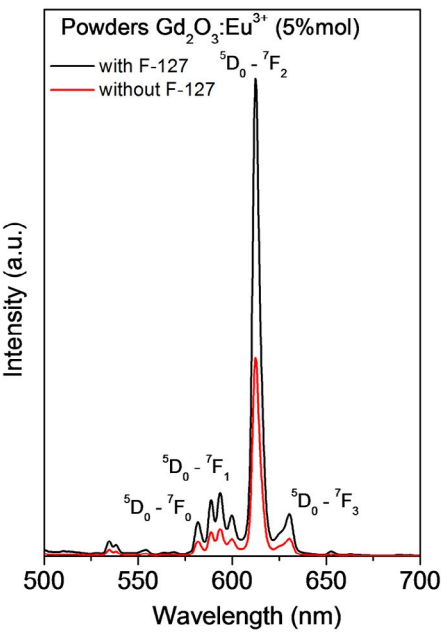

(b) comparison of the $Gd_2O_3:Eu^{3+}$ powders with and without F-127, heat-treated at 800 °C

Figure 4. PL spectra of (a) the $Gd_2O_3:Eu^{3+}$ powders synthesized in the presence of F-127 heat-treated at different temperatures and (b) comparison of the $Gd_2O_3:Eu^{3+}$ powders with and without F-127, heat-treated at 800 ºC.

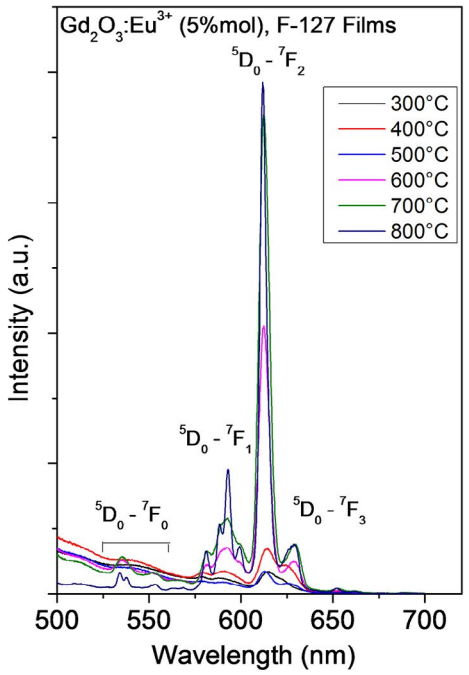

(a) $Gd_2O_3:Eu^{3+}$ films synthesized in the presence of F-127, heat-treated at different temperatures

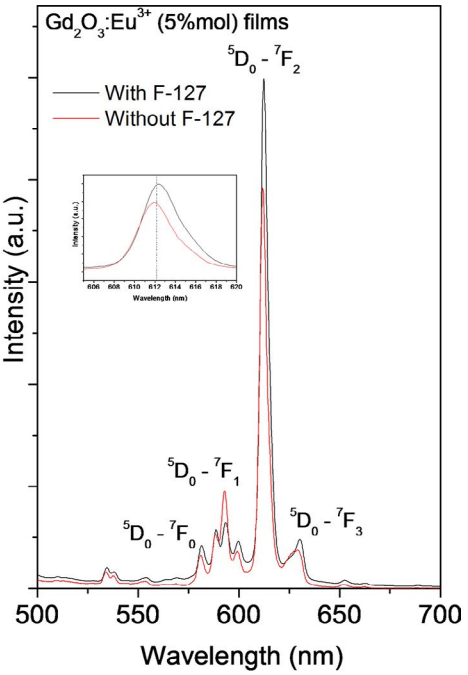

(b) comparison of the $Gd_2O_3:Eu^{3+}$ films with and without F-127, heat-treated at 800 °C

Figure 5. PL spectra of (a) the $Gd_2O_3:Eu^{3+}$ films synthesized in the presence of F-127, heat-treated at different temperatures and (b) comparison of the $Gd_2O_3:Eu^{3+}$ films with and without F-127, heat-treated at 800 ºC.

Pluronic F-127 affected the structure and crystalline size of the as-prepared modified films. F-127 is a hydrophilic, non-toxic copolymer with a micellar structure that improves its aqueous dispersity; it plays an effective role in controlling hydrolysis and condensation reactions. In the case of the Gd_2O_3:Eu^{3+}-modified films, thermal treatment up to 800 ºC may result in a destructive effect on the final phases, allowing for the formation of monoclinic nanocrystallites that induce a residual stress [40]. Finally, other factors may explain the differences in the PL emission intensity, depending on the crystal size [41,42]. Some authors have reported variations in the emission intensity of doped nanocrystalline phosphors [43] and optical properties, due to a reduction in the size of particles in the nano-range scale [44,45]. They observed that a decrease in the particle size of doped nanocrystalline systems increases the intensity of PL emissions. This is because the decrease in size causes the exciton wave functions to overlap with those of the doping ions, enhancing the energy transfer rate from the excitons to the doping ions. This, in turn, reduces the non-radiative decay rate and increases the PL emission intensity [46]. Small crystallites promote a non-radiative de-excitation process, due to the larger number of atoms on the nanoparticles' surface, unlike larger particles, favoring a Eu^{3+} red emission [47].

4. Conclusion

Gd_2O_3:Eu^{3+} powders and films modified and synthesized in the presence of F-127 were prepared by the sol-gel method. The synthesized ceramics exhibit both structural and improved luminescence compared to those of non-modified systems. Europium-active cubic powder and oriented films in the presence of F-127 are characterized by small crystallites of 19 and 15 nm, respectively, after 800 ºC thermal treatment. The results show that a portion of cubic Gd_2O_3 transforms into the monoclinic phase. Nevertheless, at a 254-nm excitation of the Gd_2O_3 host, the monoclinic portion was ineffective, but led mainly to the characteristic emission of Eu^{3+} associated with a cubic structure. Luminescence analyses showed an improved emission from modified Gd_2O_3:Eu^{3+} in both powders and crack-free films due to the F-127 surfactant and a superior densification process. These modified, europium-active and F-127-modified films show promise for phosphors on which display technologies are based.

5. Acknowledgments

The authors gratefully acknowledge the financial support of this work by the SIP-IPN projects 20196322 and 20196329 and by CNMN-IPN experimental support. Victor H. Colín Calderón acknowledges the Conacyt Ms S scholarship. The authors also would like to thank Henry Jankiewicz for the editing work that he did for this paper and M. García Murillo for her assistance.

6. References

1. Wang J, Lu Q, Liu Q. Synthesis and luminescence properties of Eu or Tb doped Lu_2O_3 square nanosheets. *Optical Materials*. 2007;29(6):593-597.

2. Huang SH, Xu J, Zhang Z, Wang L, Gai S, He F, et al. Rapid, morphologically controllable, large-scale synthesis of uniform $Y(OH)_3$ and tunable luminescent properties of Y_2O_3:Yb^{3+}/Ln3+ (Ln = Er, Tm and Ho). *Journal of Materials Chemistry*. 2012;22(31):16136-16144.

3. Yang L, Wang J, Dong XT, Liu G, Yu W. Synthesis of Y_2O_2S:Eu^{3+} luminescent nanobelts via electrospinning combined with sulfurization technique. *Journal of Materials Science.* 2013;48(2):644-650.

4. Kim GC, Mho SI, Park HL. Observation of energy transfer between Ce^{3+} and Eu^{3+} in $YAlO_3$:Ce, Eu. J*ournal of Materials Science Letters*. 1995;14(11):805-806.

5. Choe JY, Ravichandran D, Biomquist SM, Morton DC, Kirchner KW, Ervin MH, et al. Alkoxy sol-gel derived $Y_{3-x}Al_5O_{12}$:Tb_x thin films as efficient cathodoluminescent phosphors. *Applied Physics Letters*. 2001;78(24):3800-3803.

6. Ozawa L. Crts are forever as video display devices. *Materials Chemistry and Physics*. 1997;51(2):107-113.

7. Chen H, Xu C, Chen C, Zhao G, Liu Y. Flower-like hierarchical nickel microstructures: Facile synthesis, growth mechanism, and their magnetic properties. *Materials Research Bulletin*. 2012;47(8):1839-1844.

8. Vu HHT, Atabaev TS, Kim YD, Lee JH, Kim HK, Hwang YH. Synthesis and optical properties of Gd_2O_3:Pr^{3+} phosphor particles. *Journal of Sol-Gel Science and Technology*. 2012;64(1):156-161.

9. Dhananjaya N, Nagabhushana H, Nagabhushana BM, Chakradhar RPS, Shivakumara C, Rudraswamy B. Synthesis, characterization and photoluminescence properties of Gd2O3:Eu3+ nanophosphors prepared by solution combustion method. *Physica B: Condensed Matter*. 2010;405(17):3795-3799.

10. Zhydachevskyy Y, Tsiumra V, Baran M, Lipinska L, Sybilski P, Suchocki A. Quantum efficiency of the down-conversion process in Bi^{3+}-Yb^{3+} co-doped Gd_2O_3. Journal of Luminescence. 2018;196:169-173.

11. Lin KM, Lin CC, Li YY. Luminescent properties and characterization of Gd_2O_3:Eu^{3+}@SiO_2 and $Gd_2Ti_2O_7$:Eu^{3+}@SiO_2 core-shell phosphors prepared by a sol-gel process. *Nanotechnology*. 2006;17(6):1745-1751.

12. García-Murillo A, Le Luyer C, Dujardin C, Pédrini C, Mugnier J. Elaboration and characterization of Gd_2O_3 waveguiding thin films prepared by the sol-gel process. *Optical Materials*. 2001;16(1-2):39-46.

13. Ou M, Mutelet B, Martini M, Bazzi R, Roux S, Ledoux G, et al. Optimization of the synthesis of nanostructured Tb^{3+}-doped Gd_2O_3 by in-situ luminescence following up. *Journal of Colloid and Interface Science*. 2009;333(2):684-689.

14. Maalej NM, Qurashi A, Assadi AA, Maalej R, Shaikh MN, Ilyas M, et al. Synthesis of Gd_2O_3:Eu nanoplatelets for MRI and fluorescence imaging. *Nanoscale Research Letters*. 2015;10(2015):215-225.

15. Yang J, Li C, Chen Z, Zhang X, Quan Z, Zhang C, et al. Size-Tailored Synthesis and Luminescent Properties of One-Dimensional Gd_2O_3:Eu^{3+} Nanorods and Microrods. *The Journal of Physical Chemistry C*. 2007;111(49):18148-18154.

16. Li YB, Bando Y, Golberg D. M_oS_2 Nanoflowers and Their Field-Emission Properties. *Applied Physics Letters*. 2003;82(12):1962-1964.

17. Wawrzynczyk D, Nyk M, Bednarkiewicz A, Strek W, Samoc M. Morphology- and size-dependent spectroscopic properties of Eu^{3+}-doped Gd_2O_3 colloidal nanocrystals. *Journal of Nanoparticle Research*. 2014;16(11):2690.

18. Benhebal H, Bendrabah B, Ammari A, Madoune Y, Lambert SD. Structural and optoelectronic properties of SnO_2 thin films doped by group-IA elements. *Surface Review and Letters*. 2017;24(Suppl 1):1850007.

19. Liu X, Zhou F, Gu M, Huang S, Liu B, Ni C. Fabrication of highly a-axis-oriented Gd_2O_3:Eu^{3+} thick film and its luminescence properties. *Optical Materials*. 2008;31(2):126-130.

20. García-Murillo A, Le Luyer C, Garapon C, Dujardin C, Bernstein E, Pedrini C, et al. Optical properties of europium-doped Gd_2O_3 waveguiding thin films prepared by the sol-gel Method. *Optical Materials*. 2002;19(1):161-168.

21. Cho MH, Ko DH, Jeong K, Whangbo SW, Whang CN, Choi SC, et al. Growth stage of crystalline Y_2O_3 film on Si(100) grown by an ionized cluster beam deposition. *Journal of Applied Physics*. 1999;85(5):2909-2914.

22. Nicolas D, Masenelli B, Mélinon P, Bernstein E, Dujardin C, Ledoux G, et al. Structural transition in rare earth oxide clusters. *The Journal of Chemical Physics*. 2006;125(17):171104.

23. Gao S, Lu H, Nie Y, Chen H, Xu D, Dai Q, et al. Structural transition induced by the release of residual stress in the complex of cubic and monoclinic Gd_2O_3:Eu nanoparticles. *Materials Letters*. 2007;61(18):4003-4005.

24. Shannon RD, Prewitt CT. Effective ionic radii in oxides and fluorides. *Acta Crystallographica B*. 1976;25(5):925-946.

25. Alammar T, Cybinska J, Campbell PS, Mudring AV. Sonochemical synthesis of highly luminescent Ln_2O_3:Eu^{3+} (Y, La, Gd) nanocrystals. *Journal of Luminescence*. 2016;169(Pt B):587-593.

26. Langford JI, Delhez R, de Keijser TH, Mittemeijer EJ. Profile Analysis for Microcrystalline Properties by the Fourier and Other Methods. *Australian Journal of Physics*. 1988;41(2):173-187.

27. Solís D, López-Luke T, de la Rosa E, Salas P, Angeles-Chavez C. Surfactant effect on the upconversion emission and decay time of ZrO_2:Yb-Er nanocrystals. *Journal of Luminescence*. 2009;129(5):449-455.

28. Zhang S, Jiang F, Qu G, Lin C. Synthesis of single-crystalline perovskite barium titanate nanorods by a combined route based on sol-gel and surfactant-templated methods. *Materials Letters*. 2008;62(15):2225-2228.

29. Wu YC, Parola S, Marty O, Mugnier J. Elaboration, structural characterization and optical properties of the yttrium alkoxide derived Y_2O_3 planar optical waveguides. *Optical Materials*. 2004;27(1):2127.

30. Kim YK, Kim HK, Kim DK, Cho G. Synthesis of Eu-doped $(Gd,Y)_2O_3$ transparent optical ceramic scintillator. *Journal of Materials Research*. 2004;19(2):413-416.

31. Nidhi R, Yadav I, Ahlawat DS, Aghamkar P. Concentration dependent structural behavior of Gd_2O_3 nanocrystallites dispersed in silica matrix. *Journal of Optoelectronics and Advanced Materials*. 2015;17(5-6):640-645.

32. Weng W, Yang J, Ding Z. The sol-gel process of the yttrium complex from yttrium acetate. *Journal of Non-Crystalline Solids*. 1994;169(1-2):177-182.

33. Jia G, You H, Liu K, Zheng Y, Guo N, Zhang H. Highly Uniform Gd_2O_3 Hollow Microspheres: Template-Directed Synthesis and Luminescence Properties. *Langmuir*. 2010;26(7):5122-5128.

34. Morales Ramírez AJ, García Hernández M, García Murillo A, Carrillo Romo FJ, Moreno Palmerin J, Medina Velázquez DY, et al. Structural and Luminescence Properties of Lu_2O_3:Eu^{3+} F127 Tri-Block Copolymer Modified Thin Films Prepared by Sol-Gel Method. *Materials*. 2013;6(3):713-725.

35. Stathatos E, Lianos P, Tsakiroglou C. Highly efficient nanocrystalline titania films made from organic/inorganic nanocomposite gels. *Microporous and Mesoporous Materials*. 2004;75(3):255-260.

36. Dag Ö, Soten I, Çelik Ö, Polarz S, Coombs N, Ozin GA. Solventless Acid-Free Synthesis of Mesostructured Titania: Nanovessels for Metal Complexes and Metal Nanoclusters. *Advanced Functional Materials*. 2003;13(1):30-36.

37. Choi H, Stathatos E, Dionysiou DD. Synthesis of nanocrystalline photocatalytic TiO_2 thin films and particles using sol-gel method modified with nonionic surfactants. *Thin Solid Films*. 2006;510(1-2):107-114.

38. Szczyrbowski J, Czapla A. Optical absorption in D.C. sputtered InAs films. *Thin Solid Films*. 1977;46(2):127-137.

39. Seo S, Yang H, Holloway PH. Controlled shape growth of Eu- or Tb-doped luminescent Gd_2O_3 colloidal nanocrystals. *Journal of Colloid and Interface Science*. 2009;331(1):236-242.

40. Chen HY, He CY, Gao CX, Zhang JH, Gao SY, Lu HL, et al. Structural Transition of Gd_2O_3:Eu Induced by High Pressure. *Chinese Physics Letters*. 2007;24(1):158-160.

41. Boukerika A, Guerbous L. Annealing effects on structural and luminescence properties of red Eu^{3+}-doped Y_2O_3 nanophosphors prepared by sol-gel method. *Journal of Luminescence*. 2014;145:148-153.

42. Lakshminarasimhan N, Varadaraju UV. Role of crystallite size on the photoluminescence properties of $SrIn_2O_4$:Eu^{3+} phosphor synthesized by different methods. *Journal of Solid State Chemistry*. 2008;181(9):2418-2423.

43. Goldburt ET, Kulkarni B, Bhargava RN, Taylor J, Libera M. Variation of Luminescent Efficiency With Size of Doped Nanocrystalline Y_20_3:Tb Phosphor. *MRS Proceedings*. 1996;424:441.

44. Ammari A, Trari M, Bellal B, Zebbar N. Effect of Sb doping on the transport and electrochemical properties of partially amorphous SnO_2 thin films. *Journal of Electroanalytical Chemistry*. 2018;823:638-646.

45. Ammari A, Trari M, Zebbar N. Transport properties in Sb-doped SnO_2 thin films: Effect of UV illumination and temperature dependence. *Materials Science in Semiconductor Processing*. 2019;89:97-104.

46. Bhargava RN, Gallagher D, Hong X, Nurmikko A. Optical properties of manganese-doped nanocrystals of ZnS. *Physical Review Letters*. 1994;72(3):416-419.

47. Wang WN, Widiyastuti W, Ogi T, Lenggoro W, Okuyama K. Correlations between Crystallite/Particle Size and Photoluminescence Properties of Submicrometer Phosphors. *Chemistry of Materials*. 2007;19(7):1723-1730.